Biochemical and Biophysical Research Communications 496 (2018) 562–567

Contents lists available at ScienceDirect

Biochemical and Biophysical Research Communications

journal homepage: www.elsevier.com/locate/ybbrc

Structural insights into K48-linked ubiquitin chain formation by the Pex4p-Pex22p complex

Matthew R. Groves [a], Carsten F.E. Schroer [b], Adam J. Middleton [c], Sergey Lunev [a], Natasha Danda [d, 1], Ameena M. Ali [a], Siewert J. Marrink [b], Chris Williams [d, *]

[a] Department of Drug Design, Groningen Research Institute of Pharmacy, University of Groningen, 9713AV, The Netherlands
[b] Molecular Dynamics, Groningen Biomolecular Sciences and Biotechnology Institute, University of Groningen, 9747AG, The Netherlands
[c] Department of Biochemistry, School of Biomedical Sciences, University of Otago, Dunedin 9054, New Zealand
[d] Molecular Cell Biology, Groningen Biomolecular Sciences and Biotechnology Institute, University of Groningen, 9747AG, The Netherlands

ARTICLE INFO

Article history:
Received 12 December 2017
Accepted 24 December 2017
Available online 28 December 2017

Keywords:
Pex4
Pex22
Peroxisome
Ubiquitin conjugating enzyme
Ubiquitination

ABSTRACT

Pex4p is a peroxisomal E2 involved in ubiquitinating the conserved cysteine residue of the cycling receptor protein Pex5p. Previously, we demonstrated that Pex4p from the yeast *Saccharomyces cerevisiae* binds directly to the peroxisomal membrane protein Pex22p and that this interaction is vital for receptor ubiquitination. In addition, Pex22p binding allows Pex4p to specifically produce lysine 48 linked ubiquitin chains *in vitro* through an unknown mechanism. This activity is likely to play a role in targeting peroxisomal proteins for proteasomal degradation.

Here we present the crystal structures of Pex4p alone and in complex with Pex22p from the yeast *Hansenula polymorpha*. Comparison of the two structures demonstrates significant differences to the active site of Pex4p upon Pex22p binding while molecular dynamics simulations suggest that Pex22p binding facilitates active site remodelling of Pex4p through an allosteric mechanism. Taken together, our data provide insights into how Pex22p binding allows Pex4p to build K48-linked Ub chains.

1. Introduction

Peroxisomal matrix protein import in yeast requires the ubiquitin-conjugating enzyme (UBC or E2) Pex4p [1]. Pex4p, together with a complex consisting of the RING E3 ligases Pex2p, Pex10p and Pex12p, ubiquitinates the receptor proteins Pex5p [2,3] and members of the Pex20p co-receptor family [4,5]. This modification, which occurs on a conserved cysteine residue in Pex5p/Pex20 proteins [5,6], facilitates receptor recycling from the peroxisomal membrane [7,8]. Pex4p interacts with the peroxisomal membrane protein Pex22p [9] and it was proposed that Pex22p allows Pex4p to associate with the peroxisomal membrane. Later, reports showed that Pex22p binding is required for Pex4p to ubiquitinate Pex5p [10,11], possibly for positioning the active site of Pex4p close to the cysteine in Pex5p, to allow ubiquitin (Ub) transfer [11].

In addition to a role in Pex5p ubiquitination, we previously demonstrated that Pex22p from the yeast *Saccharomyces cerevisiae* (Sc) allows ScPex4p to build lysine 48 (K48)-linked Ub chains *in vitro*, in an E3 ligase-independent manner [11,12]. Hence, ScPex22p binding can alter the activity profile of ScPex4p. The function of this acquired activity is unclear, but may suggest that ScPex22p allows ScPex4p to modify peroxisomal proteins with K48-linked Ub chains, to target them for proteasomal degradation. Indeed, several reports suggest a role for Pex4p in protein degradation [5,13,14]. Therefore, insights into how Pex22p allows Pex4p to produce K48-linked Ub chains will increase our understanding of the role of Pex4p in peroxisome biology.

The ScPex22p binding site in ScPex4p is distant from the active site [11]. This could suggest that ScPex22p binding allows ScPex4p to build K48-linked Ub chains through an allosteric mechanism. However, because we have been unable to obtain the structure ScPex4p alone [11], the molecular details of such a mechanism remain elusive. Therefore, to provide insights into this mechanism, we have turned to Pex4p and Pex22p from the yeast *Hansenula polymorpha* (Hp). In this report, we show that the HpPex4p-HpPex22p complex also produces K48-linked Ub chains *in vitro*,

* Corresponding author.
E-mail address: c.p.williams@rug.nl (C. Williams).
[1] Current address: Institut du Cerveau et de la Moelle épinière (ICM), Hôpital Pitié-Salpêtrière, 47 bd de l'Hôpital, 75013 Paris, France.

https://doi.org/10.1016/j.bbrc.2017.12.150

indicating that this property is conserved. We report the crystal structures of HpPex4p alone and in complex with the soluble region of HpPex22p, observing significant differences to the active site of HpPex4p in the two structures. Furthermore, molecular dynamics (MD) simulations demonstrate that binding of HpPex22p to HpPex4p can allosterically remodel the HpPex4p active site environment. Finally, we discuss the role of active site remodelling in K48-linked Ub chain formation.

2. Materials and methods

2.1. Construction of plasmids and strains

Escherichia coli vectors for expression of His_6-GST tagged full length HpPex4p (hereafter Pex4p) and the truncated version of HpPex22p lacking the transmembrane domain (consisting of residues 26–160, hereafter $Pex22^S$) are described in (Ali et al. 2018 [33]).

2.2. Protein expression and purification

Pex4p and $Pex22^S$ were expressed and purified as described in (Ali et al. 2018 [33]). *E. coli* cell pellets expressing His_6-GST tagged proteins were lysed with a French press in buffer 1 (50 mM Tris-HCl, 300 mM NaCl, 1 mM β-mercaptoethanol, pH7.5) and cleared lysates were loaded onto glutathione sepharose-4B beads (GE Healthcare). Beads were sequentially washed with buffer1, buffer2 (50 mM Tris, 1 M NaCl, 1% Glycerol and 1 mM β-mercaptoethanol, pH7.5) and buffer3 (50 mM Tris, 150 mM NaCl, 1% Glycerol and 1 mM β-mercaptoethanol, pH7.5) and His_6-GST tagged proteins were eluted in buffer3 containing 20 mM reduced glutathione. His_6GST tags were removed by cleavage with His_6-TEV and proteins were further purified by gel filtration on a Superdex 75 (16/60) column equilibrated with 25 mM Tris, 150 mM NaCl, 1% glycerol, 1 mM β-mercaptoethanol, pH7.4.

The Human E1 (Ube1) was expressed and purified as described [15], while the E51R, D58A and Y59L mutant forms of Ub were produced as in Ref. [16].

2.3. In vitro ubiquitination reactions

Reactions were performed at 35 °C in 25 mM Tris, 75 mM NaCl, 5 mM $MgCl_2$, pH8 with shaking and contained: human E1 (0.3 μM), WT or K48R (R&D systems Europe) or other mutant Ub (15 μM), Pex4p (6 μM) and $Pex22^S$ (6 μM). Reactions were initiated by the addition of ATP (5 mM) and samples were taken at the time points indicated. Reactions were quenched with loading buffer containing 5% β–mercaptoethanol and analysed by SDS-PAGE and coomassie staining.

2.4. Crystallization, X-ray data collection and structure determination

Crystals of Pex4p and the Pex4p-$Pex22^s$ complex (both at 12 mg/ml) were obtained using hanging drop vapour diffusion at 20 °C (Ali et al. 2018 [33]). Pex4p alone crystalized in 100 mM MES pH6.5, 50% (v/v) PEG-200 while the Pex4p-$Pex22^S$ complex crystallized in 200 mM sodium sulphate pH7.8, 100 mM BIS-TRIS Propane, 22% w/v PEG-3350. Cryo-protectant was the crystallization buffer including 20% (v/v) glycerol. Single wavelength datasets were collected on crystals and processed using XDS/XDSAPP [17]. The structure of Pex4p alone was solved by molecular replacement using MOLREP [18], using the coordinates of ScPex4p 2y9m as search model, while the structure of the Pex4p-$Pex22^S$ complex was solved using a model built from the structure of Pex4p together with $ScPex22^S$ from the ScPex4p-$Pex22^S$ structure (2y9m). In both cases, the region around the active site (residues 118–123) was removed from the model and build by hand, to avoid model bias. Subsequent cycles of refinement with REFMAC [19] and rebuilding in COOT [20] resulted in high quality structural models.

2.5. Accession numbers

Coordinates and structure factors of Pex4p alone (5NL8) and the Pex4p-$Pex22^S$ complex (5NKZ) have been deposited in the Protein Data Bank.

2.6. Molecular dynamics simulations

MD simulations were conducted with GROMACS 5.0.7 [21] using the united atom force field GROMOS 54A7 [22]. Two different systems were used: the structure of Pex4p alone and Pex4p docked to $Pex22^S$ at the binding site. Structures were placed in a dodecahedral box with an edge length of 7.6 nm for Pex4p alone and 9.8 nm for the docked complex. The molecules were eventually solvated with single point charge (SPC) water [23] containing 0.15 M NaCl. After energy minimization, the system was equilibrated for 10 ps at 200K under constant number, volume and temperature (NVT) conditions using harmonic constraints to keep the position of the protein atoms fixed. Subsequently, a production run of 510ns in case ofpPex4p alone and 920ns for the complex was performed at 300K under constant pressure (NPT) conditions without constraints. The temperature of the system in the equilibration phase was controlled via the Berendsen algorithm [24] with a relaxation time of 0.1ps, in the production phase via the Nosé-Hoover thermostat [25,26] with a relaxation time of 0.5ps. Isotropic pressure coupling was applied with a reference pressure of 1 bar and a relaxation time of 2.0ps using the Berendsen barostat. The integration time step in all cases was 2fs. Non-bonded interactions were calculated up to 1.2 nm using a neighbour list that was updated every 5 integration steps. Long-range electrostatic interactions were included with the Particle Mesh Ewald method [27]. MDAnalysis [28,29] was used to conduct the distance analysis presented.

3. Results and discussion

3.1. Pex22p binding allows Pex4p to build K48-linked Ub chains

H. polymorpha Pex4p and Pex22p display 31 and 15% identity and 60 and 51% similarity with their *S. cerevisiae* counterparts, respectively (Figs. S1A and B). Previously we demonstrated that full length Pex4p can bind to $Pex22^S$ *in vitro*, with the interaction displaying a dissociation constant of 1.94 ± 0.39 nM (Ali et al. 2018 [33]). To test whether purified Pex4p was active, we performed E2 self-ubiquitination assays. Reactions contained E1, Pex4p, Ub and ATP and were probed with SDS-PAGE and coomassie staining. Before addition of ATP, Pex4p runs as a discreet band of ~22 kDa (Fig. 1A). Addition of ATP resulted in the disappearance of Pex4p and the formation of a prominent band of ~30 kDa, which corresponds well with the predicted molecular weight of Pex4p modified with a single Ub molecule of ~8.6 kDa. Inclusion of $Pex22^S$ resulted in the formation of a "ladder" of modified proteins (Fig. 1A). The molecular weight of the four species directly above Pex4-Ub_1 in Fig. 1A corresponds well with those predicted for Pex4p modified with respectively 2 (~39 kDa), 3 (~47 kDa), 4

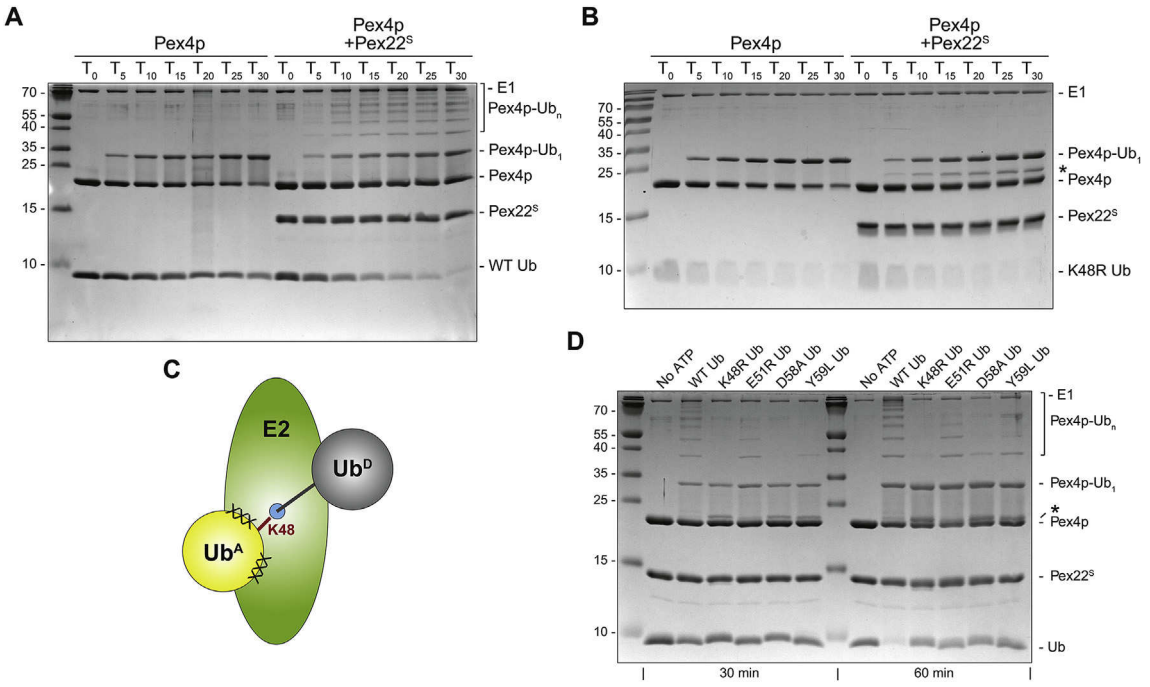

Fig. 1. The Pex4p-Pex22^S complex builds K48-linked Ub chains. (A) *In vitro* ubiquitination reaction containing E1, Pex4p, ATP, Ub with or without Pex22^S, analysed by SDS-PAGE and coomassie staining. Samples were taken at the indicated time (in minutes) after addition of ATP. (B) *In vitro* ubiquitination reaction performed and analysed as in (A) but containing K48R Ub. * depicts ubiquitinated Pex22^S. (C) Schematic representation of an E2 poised to transfer donor ubiquitin (Ub^D) from its active site (cyan) to K48 (red) in an acceptor ubiquitin (Ub^A). Crosses depict contacts between the E2 and Ub^A. (D) *In vitro* ubiquitination reactions performed for thirty (left) or sixty minutes (right) containing WT or mutant forms of Ub, analysed by SDS-PAGE and coomassie staining. * depicts ubiquitinated Pex22^S. (For interpretation of the references to colour in this figure legend, the reader is referred to the Web version of this article.)

(~56 kDa) or 5 (~64 kDa) Ub molecules, leading us to conclude that these represent multiply ubiquitinated forms of Pex4p.

Because ScPex22^S allows ScPex4p to produce K48-linked Ub chains *in vitro* [11], we investigated whether the multiply ubiquitinated forms of Pex4p contained K48-linked Ub chains. Inclusion of K48R Ub in reactions blocked the formation of multiply ubiquitinated forms of Pex4p (Fig. 1B), indicating that Pex22^S can indeed induce Pex4p to produce K48-linked Ub chains. Inclusion of K48R Ub also resulted in the formation an extra band of around 23 kDa (Fig. 1B, asterisks), which we confirmed to be ubiquitiated Pex22^S using mass spectrometry (Fig. S2). It is possible that under these circumstances Pex22^S becomes a target for Ub conjugation because K48 in Ub is no longer available.

Although a unified mechanism for K48-linked Ub chain formation has not been defined [16], contacts between the E2 active site environment and the "acceptor" Ub molecule (Ub^A) around K48 can play a crucial role. Such contacts allow K48 in Ub^A to approach the E2 active site cysteine and facilitate transfer of the donor Ub molecule (Ub^D) from the active site to K48 in Ub^A (Fig. 1C) [30,31]. We reasoned that because K48-linked Ub chain formation only occurs in the presence of Pex22^S, Pex22^S binding may allow Pex4p to contact Ub^A. To investigate this, we assessed whether the Pex4p-Pex22^S complex can produce Ub chains with mutant forms of Ub (E51R, D58A, Y59L) that were shown to disturb E2-Ub^A contacts [16,30,31]. Indeed Ub chain formation was inhibited by the D58A and Y59L mutations (Fig. 1D). Furthermore, similar to reactions containing K48R Ub, increased levels of Pex22^S ubiquitination were observed in reactions containing D58A and Y59L Ub (Fig. 1D, asterisk), correlating the effect caused by the Ub K48R and D58A/Y59L mutants.

Taken together, our data establish that the *H. polymorpha* Pex4p-Pex22^S complex can produce K48-linked Ub chains while also suggesting that Pex22^S binding allows Pex4p to contact the region around K48 in Ub^A.

3.2. Crystal structures of Pex4p alone and in complex with Pex22^S

To gain molecular insights into how Pex22^S allows Pex4p to produce K48-linked Ub chains, we solved the crystal structures of Pex4p alone and in complex with Pex22^S (Fig. 2 and Table 1). Pex4p alone crystallized with a single molecule in the asymmetric unit, whereas crystals of the complex displayed two near identical Pex4p-Pex22^S complexes in the asymmetric unit. With the exception of the N- and C-termini, Pex4p is complete in both structures (Fig. S1C). Pex4p adopts a UBC fold, consisting of a central domain of four anti-parallel β-strands (β1–β4), an N-terminal helix (α1), two C-terminal helices (α3–α4) and one α-helix (α2) that packs against the central β-sheet domain (Fig. 2C and Fig S1C). Additional secondary structure elements include two α-helices, one directly following helix α1 (α′) and the other following β4 (α"). A pair of β-strands (β5 and β6) that assemble close to the α" helix are also present in the structure of Pex4p alone (Fig. S1C). In addition, Pex4p alone does not contain a 3_{10} helix following the active site cysteine (C119), an element common in many E2s [32]. Instead, residues Leu120-Lys126 form an α-helix (α*). When in complex with Pex22^S this helix partially unfolds, with residues Asp121-Leu123 forming a 3_{10} helix (Fig. 2C and Fig S1C).

Interpretable electron density for residues 50–155 of Pex22^S was visible, while electron density for residues 26–49 and 156–160 was not, presumably due to disorder. Residues 50–155 of Pex22^S form a central β-sheet, consisting of four parallel β-strands, sandwiched by seven α-helices (Fig. S1C). Pex4p binds to Pex22^S in a similar manner to that seen in the ScPex4p-ScPex22^S complex (Fig. S3). The Pex22^S interface in Pex4p is formed by residues from the helices α3 and α4 and involves both hydrophobic and polar contacts (Fig. S1A). The major Pex4p binding site in Pex22^S consists

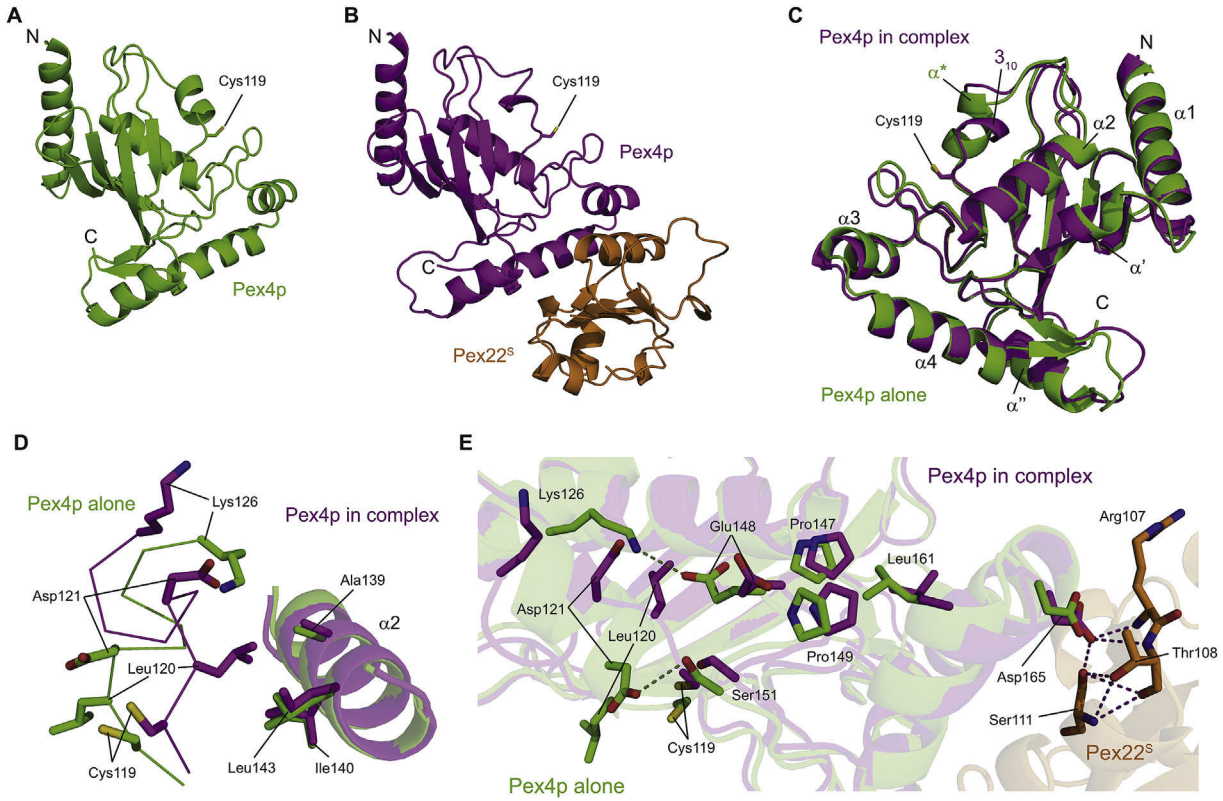

Fig. 2. Structures of Pex4p alone and the Pex4p-Pex22^S complex. Crystal structures of Pex4p alone (A) and Pex4p in complex with Pex22^S (B), indicating the N- and C-termini and the active site cysteine (Cys119). (C) Structural alignment of Pex4p alone (green) and Pex4p (magenta) when in complex with Pex22^S (not shown) indicating α-helices and the active site (Cys119). (D and E) Residues in Pex4p (colours as in C) that reposition upon binding of Pex22^S (orange). Depicted are the area around the Pex4p active site (D) and the residues that lead from the Pex22^S binding site to the active site (E). Residues are depicted in stick form and numbered while hydrogen bonds are displayed as dotted lines. (For interpretation of the references to colour in this figure legend, the reader is referred to the Web version of this article.)

Table 1
Data collection and refinement statistics.

	Pex4p alone	Pex4p-Pex22^S complex
Data collection		
Space group	$P4_12_12$	$P1$
Unit-cell parameters		
a, *b*, *c* (Å)	46.4, 46.4, 206.4	44.7, 61.6, 78.4
α, β, γ (°)	90, 90, 90	89.2, 78.0, 84.1
Resolution (Å)	45.22–2.0 (2.26–2.0)[a]	76.7–2.85 (2.95–2.85)
R_{merge}	14.7% (74%)	12.3% (80%)
Mean $I/\sigma(I)$	6.21 (1.69)	6.03 (1.14)
Completeness (%)	92% (88%)	95.02 (94.5%)
Redundancy	4.13 (1.63)	3.93 (5.49)
Refinement		
Resolution (Å)	45.22–2.2	48.04–2.85
Total No. of unique reflections	11654 (2559)	19431 (2699)
R_{work}/R_{free}	0.21/0.26	0.24/0.28
Number atoms	1534	4655
Protein	1479	4655
Ion	0	0
Water	55	0
B factors	44.2	63.4
R.m.s. deviation		
Bond length (Å)	0.022	0.016
Bond angle (°)	2.234	1.925

Each dataset was collected from a single crystal.
[a] Values in parentheses are for highest-resolution shell.

of residues from helices α4 and α5, β-strand β3 and the loop region between β3 and α5, while residues from helix α3 and the loop region between helix α2 and β-strand 2 also contribute (Fig. S1B).

3.3. Pex22^S binding impacts on the active site of Pex4p

Pex4p does not display large structural alterations when bound

to Pex22^S (Fig. 2C). The backbone root-mean-square deviation across all Cα atoms is ~1 Å. However, prominent differences around the active site can be observed (Fig. 2D). Leu120, which is surface exposed in Pex4p alone, rotates 180° to pack against the hydrophobic residues Ala139, Ile140 and Leu143 in α2 when Pex4p is bound to Pex22^S (Fig. 2D). Asp121, which hydrogen bonds with the α2-α3 loop region residue Ser151 in Pex4p alone, also rotates when in complex with Pex22^S (Fig. 2D). These rotations result in the partial unravelling of helix α*, converting it to the 3_{10} helix seen in the Pex22^S bound structure (Fig. 2C).

Our structural alignments suggest a mechanism in which Pex22^S binding remodels the active site of Pex4p allosterically, through subtle repositioning of a network of residues leading from the Pex22^S binding site to the active site environment (Fig. 2E). Asp165 in the α3-α4 loop region of Pex4p contacts the main chain atoms of Arg107 and Thr108 and the side chain Ser111 in Pex22^S (Fig. 2E). This draws Leu161 in the α3 helix of Pex4p towards Pex22^S. Leu161 makes hydrophobic contacts with Pro147 and Pro149, present in the α2-α3 loop region. The repositioning of this loop results in a loss of the Glu148-Lys126 and Ser151-Asp121 hydrogen bonds, which in turn allows Leu120 and Asp121 to reposition (Fig. 2D and E). To investigate whether this mechanism could account for the structural differences observed in the two Pex4p structures, we conducted MD simulations. We docked the structure of Pex4p alone onto Pex22^S (Fig. 3A) and compared its behaviour against Pex4p alone (Fig. 3B).

A key step in remodelling would involve breaking the hydrogen bond between Glu148 and Lys126 in Pex4p (Fig. 2E). At the start of our simulations, this hydrogen bond is present in both structures (Fig. 3A and B). However, during the first 400 nanoseconds (ns) of the simulation the distance between Glu148 and Lys126 in the docked structure fluctuates between two states (Fig. 3D), indicating that the hydrogen bond between these resides becomes labile. This behaviour was not apparent with Pex4p alone (Fig. 3D). At t = 491ns we observed a sudden increase in the distance between these two residues in the docked structure (Fig. 3A and D), caused by Glu148 bending towards the Pex22^S binding site (Fig. 3A and C). This event appears to be irreversible, since the original positioning is not recovered during the remaining simulation time (Fig. 3D). Another crucial event during remodelling is the concerted motion of Glu148 and Leu161, mediated by hydrophobic contacts between Leu161 and Pro147/Pro149, which flank Glu148 in the α2-α3 loop. We evaluated the distance between the backbone atoms of Lys126 and Leu161 in the two simulations over time. We chose the former residue as a reference since it does not change its absolute position significantly during Glu148 bending (Fig. 3C). The intermolecular distance between Lys126 and Leu161 also displays a sudden increase at t = 491ns, similar to the Lys126-Glu148 pair (Fig. 3E). However, the distance between Leu161 and Pro147/Pro149 in both simulations does not change (Fig. 3F). This demonstrates that the Leu161-Pro147/Pro149 triad moves as a single unit, acting as a connecting rod that allows a signal to be transferred from the Pex22^S binding site to the active site of Pex4p.

In conclusion, our structural and MD simulation data suggest that Pex22^S binding can induce Pex4p active site remodelling through an allosteric mechanism while our biochemical data demonstrate that Pex22p binding allows Pex4p to build K48-linked Ub chains. These results advocate a model where Pex22^S-dependent active site remodelling creates a binding platform for the region around K48 of Ub^A at the Pex4p active site, facilitating the formation of K48-linked Ub chains. Such a model suggests that Pex4p alone is unable to engage Ub^A, which may explain why Pex4p alone does not produce K48-linked Ub chains. Interestingly, the positions of Leu120 and Asp121, the residues that display the largest conformational changes upon Pex22^S binding (Fig. 2D), may be restrictive to an approaching Ub^A molecule in the structure of Pex4p alone, but not when Pex4p is in complex with Pex22^S (Fig. 4), which may support this conclusion. However, further studies will

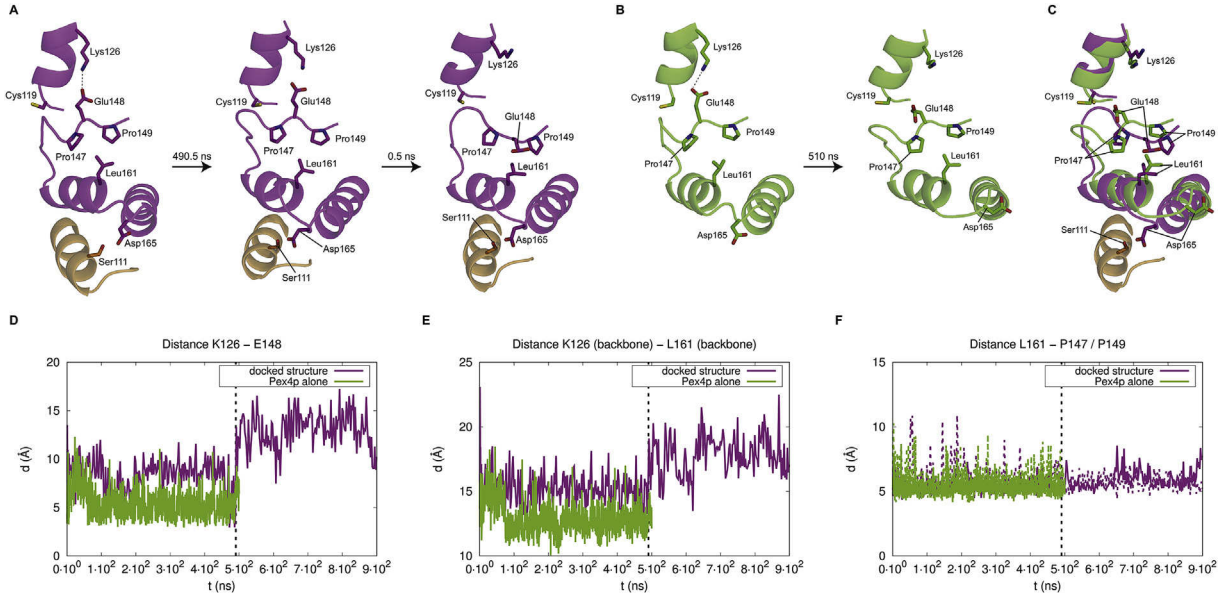

Fig. 3. Pex22^S binding allosterically remodels Pex4p *in silico*. (A) MD simulations performed for 920ns on the structure of Pex4p alone (magenta) docked onto Pex22^S (orange). Pictures were generated at t = 0ns (left panel), t = 490.5ns (middle panel) and t = 491.0ns (right panel). The hydrogen bond between Lys126 and Glu148 is depicted as dotted line. (B) Simulations performed for 510ns on the crystal structure of Pex4p alone (green). Pictures were generated at t = 0ns (left panel) and t = 510.0ns (right panel). The dotted line denotes the Lys126-Glu148 hydrogen bond. (C) Alignment of the structures of Pex4p alone (green) and Pex4p (magenta) docked onto Pex22^S (orange) after 510ns (alone) and 491ns (docked) of MD simulation time. (D–F) Changes in intermolecular distances (in Å) over time (in ns) between the side chains of Lys126 and Glu148 (D), the backbone atoms of Lys126 and Leu161 (E) and the side chains of Lys126 and Pro147 (solid line) and Pro149 (dotted line) (F) for simulations performed on Pex4p alone (green) and the docked Pex4p-Pex22^S structure (magenta). The vertical black line indicates when bending of Glu148 can be observed. (For interpretation of the references to colour in this figure legend, the reader is referred to the Web version of this article.)

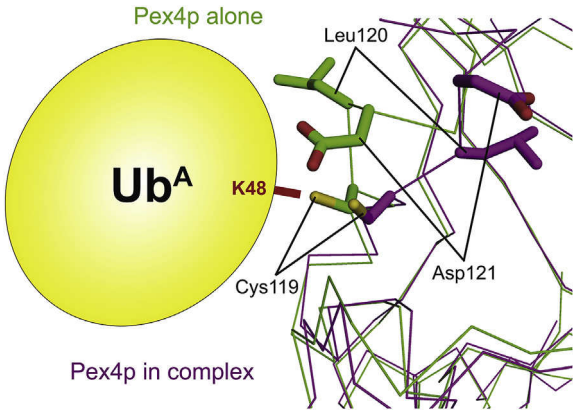

Fig. 4. Leu120 and Asp121 in Pex4p alone may inhibit contacts between Ub^A and Pex4p. Model of Pex4p alone or in complex with Pex22^S (depicted as ribbons, colours as in Fig. 2) contacting Ub^A (yellow). Cys119, Leu120 and Asp121 in Pex4p are depicted in stick representation and labelled while the suggested position of K48 of UbA (in red) is indicated. (For interpretation of the references to colour in this figure legend, the reader is referred to the Web version of this article.)

be required to validate the importance of active site remodelling in allowing the Pex4p-Pex22p complex to produce K48-linked Ub chains.

Acknowledgements

The authors gratefully acknowledge access to the beamlines P11 (DESY) and P13 (EMBL) at PETRA III (Hamburg), H. Permentier and M. Jeronimus (University of Groningen) for help with the mass spectrometry analysis, F. Sicheri (University of Toronto) for the E1 plasmid and I. J. vander Klei (University of Groningen) and M. Sattler (Technical University Munich) for advice.

This work was supported by the Netherlands Organisation for Scientific Research (NWO; grant number 723.013.004), the EMBO postdoctoral fellowship program (grant number ALTF 1340-2016) and the Qatar Research Leadership (QRLP)-Qatar Foundation.

Appendix A. Supplementary data

Supplementary data related to this article can be found at https://doi.org/10.1016/j.bbrc.2017.12.150.

Transparency document

Transparency document related to this article can be found online at https://doi.org/10.1016/j.bbrc.2017.12.150.

References

[1] F.F. Wiebel, W.H. Kunau, The Pas2 protein essential for peroxisome biogenesis is related to ubiquitin-conjugating enzymes, Nature 359 (1992) 73–76.
[2] H.W. Platta, F. El Magraoui, B.E. Baumer, D. Schlee, W. Girzalsky, R. Erdmann, Pex2 and pex12 function as protein-ubiquitin ligases in peroxisomal protein import, Mol. Cell Biol. 29 (2009) 5505–5516.
[3] A. Kragt, T. Voorn-Brouwer, M. van den Berg, B. Distel, The Saccharomyces cerevisiae peroxisomal import receptor Pex5p is monoubiquitinated in wild type cells, J. Biol. Chem. 280 (2005) 7867–7874.
[4] F. El Magraoui, R. Brinkmeier, A. Schrotter, W. Girzalsky, T. Muller, K. Marcus, H.E. Meyer, R. Erdmann, H.W. Platta, Distinct ubiquitination cascades act on the peroxisomal targeting signal type 2 co-receptor Pex18p, Traffic 14 (2013) 1290–1301.
[5] X. Liu, S. Subramani, Unique requirements for mono- and polyubiquitination of the peroxisomal targeting signal co-receptor, Pex20, J. Biol. Chem. 288 (2013) 7230–7240.
[6] C. Williams, M. van den Berg, R.R. Sprenger, B. Distel, A conserved cysteine is essential for Pex4p-dependent ubiquitination of the peroxisomal import receptor Pex5p, J. Biol. Chem. 282 (2007) 22534–22543.
[7] H.W. Platta, F. El Magraoui, D. Schlee, S. Grunau, W. Girzalsky, R. Erdmann, Ubiquitination of the peroxisomal import receptor Pex5p is required for its recycling, J. Cell Biol. 177 (2007) 197–204.
[8] S. Leon, S. Subramani, A conserved cysteine residue of Pichia pastoris Pex20p is essential for its recycling from the peroxisome to the cytosol, J. Biol. Chem. 282 (2007) 7424–7430.
[9] A. Koller, W.B. Snyder, K.N. Faber, T.J. Wenzel, L. Rangell, G.A. Keller, S. Subramani, Pex22p of *Pichia pastoris*, essential for peroxisomal matrix protein import, anchors the ubiquitin-conjugating enzyme, Pex4p, on the peroxisomal membrane, J. Cell Biol. 146 (1999) 99–112.
[10] F. El Magraoui, A. Schrotter, R. Brinkmeier, L. Kunst, T. Mastalski, T. Muller, K. Marcus, H.E. Meyer, W. Girzalsky, R. Erdmann, H.W. Platta, The cytosolic domain of Pex22p stimulates the Pex4p-dependent ubiquitination of the PTS1-receptor, PLoS One 9 (2014) e105894.
[11] C. Williams, M. van den Berg, S. Panjikar, W.A. Stanley, B. Distel, M. Wilmanns, Insights into ubiquitin-conjugating enzyme/co-activator interactions from the structure of the Pex4p:Pex22p complex, EMBO J. 31 (2012) 391–402.
[12] C. Williams, M. van den Berg, W.A. Stanley, M. Wilmanns, B. Distel, A disulphide bond in the E2 enzyme Pex4p modulates ubiquitin-conjugating activity, Sci. Rep. 3 (2013) 12.
[13] P.E. Purdue, P.B. Lazarow, Pex18p is constitutively degraded during peroxisome biogenesis, J. Biol. Chem. 276 (2001) 47684–47689.
[14] M.J. Lingard, M. Monroe-Augustus, B. Bartel, Peroxisome-associated matrix protein degradation in Arabidopsis, Proc Natl Acad Sci USA 106 (2009) 4561–4566.
[15] Y.C. Chou, A.F. Keszei, J.R. Rohde, M. Tyers, F. Sicheri, Conserved structural mechanisms for autoinhibition in IpaH ubiquitin ligases, J. Biol. Chem. 287 (2012) 268–275.
[16] A.J. Middleton, C.L. Day, The molecular basis of lysine 48 ubiquitin chain synthesis by Ube2K, Sci. Rep. 5 (2015) 16793.
[17] W. Kabsch, Xds, Acta Crystallogr D Biol Crystallogr 66 (2010) 125–132.
[18] A. Vagin, A. Teplyakov, Molecular replacement with MOLREP, Acta Crystallogr D Biol Crystallogr 66 (2010) 22–25.
[19] G.N. Murshudov, P. Skubak, A.A. Lebedev, N.S. Pannu, R.A. Steiner, R.A. Nicholls, M.D. Winn, F. Long, A.A. Vagin, REFMAC5 for the refinement of macromolecular crystal structures, Acta Crystallogr D Biol Crystallogr 67 (2011) 355–367.
[20] P. Emsley, B. Lohkamp, W.G. Scott, K. Cowtan, Features and development of coot, Acta Crystallogr D Biol Crystallogr 66 (2010) 486–501.
[21] M.J. Abraham, T. Murtola, R. Schulz, S. Páll, J.C. Smith, B. Hess, E. Lindahl, GROMACS: high performance molecular simulations through multi-level parallelism from laptops to supercomputers, Software 1–2 (2015) 19–25.
[22] N. Schmid, A.P. Eichenberger, A. Choutko, S. Riniker, M. Winger, A.E. Mark, W.F. van Gunsteren, Definition and testing of the GROMOS force-field versions 54A7 and 54B7, Eur. Biophys. J. 40 (2011) 843.
[23] H.J.C. Berendsen, J.P.M. Postma, W.F. van Gunsteren, J. Hermans, Interaction models for water in relation to protein hydration, in: B. Pullman (Ed.), Intermolecular Forces: Proceedings of the Fourteenth Jerusalem Symposium on Quantum Chemistry and Biochemistry Held in Jerusalem, Israel vol. 1981, Springer Netherlands, Dordrecht, April 13–16, 1981, pp. 331–342.
[24] H.J.C. Berendsen, J.P.M. Postma, W.F. van Gunsteren, A. DiNola, J.R. Haak, Molecular dynamics with coupling to an external bath, J. Chem. Phys. 81 (1984) 3684–3690.
[25] S. Nosé, A molecular dynamics method for simulations in the canonical ensemble, Mol. Phys. 52 (1984) 255–268.
[26] W.G. Hoover, Canonical dynamics: equilibrium phase-space distributions, Phys. Rev. 31 (1985) 1695–1697.
[27] U. Essmann, L. Perera, M.L. Berkowitz, T. Darden, H. Lee, L.G. Pedersen, A smooth particle mesh Ewald method, J. Chem. Phys. 103 (1995) 8577–8593.
[28] N. Michaud-Agrawal, E.J. Denning, T.B. Woolf, O. Beckstein, MDAnalysis: a toolkit for the analysis of molecular dynamics simulations, J. Comput. Chem. 32 (2011) 2319–2327.
[29] R.J. Gowers, M. Linke, J. Barnoud, T.J.E. Reddy, M.N. Melo, S.L. Seyler, J. Domanski, D.L. Dotson, S. Buchoux, I.M. Kenney, O. Beckstein, MDAnalysis: a Python package for the rapid analysis of molecular dynamics simulations, in: S. Benthall, S. Rostrup (Eds.), Proceedings of the 15th Python in Science Conference, 2016, pp. 98–105.
[30] M.C. Rodrigo-Brenni, S.A. Foster, D.O. Morgan, Catalysis of lysine 48-specific ubiquitin chain assembly by residues in E2 and ubiquitin, Mol Cell 39 (2010) 548–559.
[31] R.A. Chong, K. Wu, D.E. Spratt, Y. Yang, C. Lee, J. Nayak, M. Xu, R. Elkholi, I. Tappin, J. Li, J. Hurwitz, B.D. Brown, J.E. Chipuk, Z.J. Chen, R. Sanchez, G.S. Shaw, L. Huang, Z.Q. Pan, Pivotal role for the ubiquitin Y59-E51 loop in lysine 48 polyubiquitination, Proc Natl Acad Sci U S A 111 (2014) 8434–8439.
[32] F.C. Streich Jr., C.D. Lima, Structural and functional insights to ubiquitin-like protein conjugation, Annu. Rev. Biophys. 43 (2014) 357–379.
[33] A.M. Ali, J. Atmaj, A. Adawy, S. Lunev, N. Van Oosterwijk, S.R. Yan, C. Williams, M.R. Groves, Acta Cryst. F74 (2018). https://doi.org/10.1107/S2053230X17018428.